12-2008

Novel Contrast Mechanism in Cross-Sectional Scanning Tunneling Microscopy of GaSb/GaAs Type-II Nanostructures

R. Timm
Technische Universitat Berlin

Randall M. Feenstra
Carnegie Mellon University, feenstra@andrew.cmu.edu

H. Eisele
Technische Universitat Berlin

A. Lenz
Technische Universitat Berlin

L. Ivanova
Technische Universitat Berlin

See next page for additional authors

Published In
J. Appl. Phys. , 105, 093718.

Published in J. Appl. Phys. 105, 093718 (2009).

Novel Contrast Mechanism in Cross-Sectional Scanning Tunneling Microscopy of GaSb/GaAs Type-II Nanostructures

R. Timm,[1,*] R. M. Feenstra,[2] H. Eisele,[1] A. Lenz,[1] L. Ivanova,[1] E. Lenz,[3] and M. Dähne[1]

[1]*Institut für Festkörperphysik, Technische Universität Berlin, 10623 Berlin, Germany*

[2]*Department of Physics, Carnegie Mellon University, Pittsburgh, Pennsylvania, USA*

[3]*Fachgebiet für Theoretische Elektrotechnik, Technische Universität Berlin, 10587 Berlin, Germany*

(Dated: December 30, 2008)

Abstract

Cross-sectional scanning tunneling microscopy results on GaSb quantum wells and dots in GaAs are found to exhibit a narrow, sharply defined contrast of the nanostructure at negative sample bias, but a smoothly broadened contrast at positive sample bias. This novel contrast mechanism is related to the specific type-II band alignment of GaSb/GaAs heterostructures in combination with tip-induced band bending. The corresponding model is quantitatively veryfied by numerical simulations of band bending and tunnel current profiles combined with calculations of cleavage-induced strain relaxation.

PACS numbers: 68.37.Ef, 73.40.Kp, 73.63.Hs

I. INTRODUCTION

Semiconductor nanostructures are attracting widespread interest due to their unique electronic properties[1] and promising optoelectronical applications[2]. As the electronic behavior crucially depends on the size, shape, and stoichiometry of the nanostructure[3,4], the exact knowledge of such structural properties is essential both for understanding the underlying physics and for tailoring applications[5]. Cross-sectional scanning tunneling microscopy (XSTM) is a powerful tool for characterizing capped nanostructures at the atomic scale, yielding data on their structure[6–8], chemical composition[9–11], strain[12], and electronic properties[13]. Thereby the image contrast in XSTM experiments generally consists of two contributions: (1) The structural contrast is determined by the morphology of the surface including a spatial relaxation of strained nanostructures upon cleavage[12,14]. (2) The electronic contrast includes variations of the tunneling probability at heterostructures due to different bandgaps or additional confined states[12,15], standing electron waves[16], as well as effects like atom-selective imaging at different polarities[17,18] and tip-induced band bending[19,20].

Here we report on a novel XSTM image contrast mechanism which we observed studying GaSb/GaAs nanostructures, being due to a combination of tip-induced band bending and the specific band alignment in this system: Unlike the well-known InAs/GaAs system, GaSb quantum wells (QWs) and quantum dots (QDs) in GaAs exhibit a staggered type-II band alignment with a large hole confinement energy but no electron confinement within the GaSb material[21,22], making this system very interesting both for fundamental physics[23] and applications as e.g. charge storage devices[24,25].

We demonstrate that the spatial separation of holes being confined within the GaSb nanostructures and Coulomb-bound electrons in the surrounding GaAs leads to completely different tunneling conditions for different tunneling polarities. The corresponding contrast model is confirmed by a detailed computation of the tip-induced band bending and the resulting tunnel current. Furthermore, it is shown that this calculated electronic component of the image contrast together with simulations of the cleavage-induced strain relaxation can quantitatively well describe the experimental height profiles across the GaSb/GaAs QW as obtained from the XSTM data.

II. EXPERIMENTAL DETAILS

GaSb QWs were grown by L. Müller-Kirsch, U. W. Pohl, and D. Bimberg at the Technische Universität Berlin, using metalorganic chemical vapor deposition with growth conditions similar to those in Refs.[26,27]. On an n-type GaAs(001) substrate, undoped GaAs and AlGaAs buffer layers were grown, followed by 100 nm GaAs. After an interruption of 4 seconds for minimizing the As background in the reactor, nominally about 1.4 ML of pure GaSb were deposited. The QW was covered, after another growth interruption of 2 seconds, by 40 nm GaAs, 30 nm AlGaAs, and a thick n-doped GaAs cap layer.

The GaSb QD sample was fabricated by G. Balakrishnan and D. L. Huffaker at the University of New Mexico, using molecular beam epitaxy as described in detail in Refs.[28,29]. Four layers of ring-shaped QDs with increasing amount of GaSb are sandwiched in between thick undoped GaAs buffer layers grown on an n-type GaAs(001) substrate. The QDs studied in this work have been grown using a 5 s Sb soaking step followed by deposition of 2 ML GaSb.

The samples were cleaved in ultrahigh vacuum, resulting in a clean (110) cleavage surface, and analyzed by home-built scanning tunneling microscopy setups. Electrochemically etched tungsten tips were used, which were cleaned *in situ* by electron bombardment.

III. EXPERIMENTAL RESULTS

Typical images of a GaSb QW are shown in Fig. 1(a, b). The lines perpendicular to the [001] growth direction mark the atomic chains of the (110) surface, representing every second atomic monolayer[18]. The brightly appearing GaSb layer is inhomogeneous with continuous parts and small gaps filled with GaAs, which is typical for this material system[27,30]. It is also strongly intermixed: Analyzing the local lattice constant, we could determine the stoichiometry of the QW, containing only about 20% GaSb in average with a maximum of about 27% and an integrated GaSb content of about 1.0 ML[27,31].

Figures 1(a, b), showing the same QW, are taken at opposite tunneling polarity, yielding a very different appearence of the QW. In Fig. 1(a), taken at negative sample bias, the GaSb layer shows a distinctive contrast which is limited to only two or three atomic chains, as it is marked by the arrows. However, at positive sample bias, shown in Fig. 1(b), the contrast of

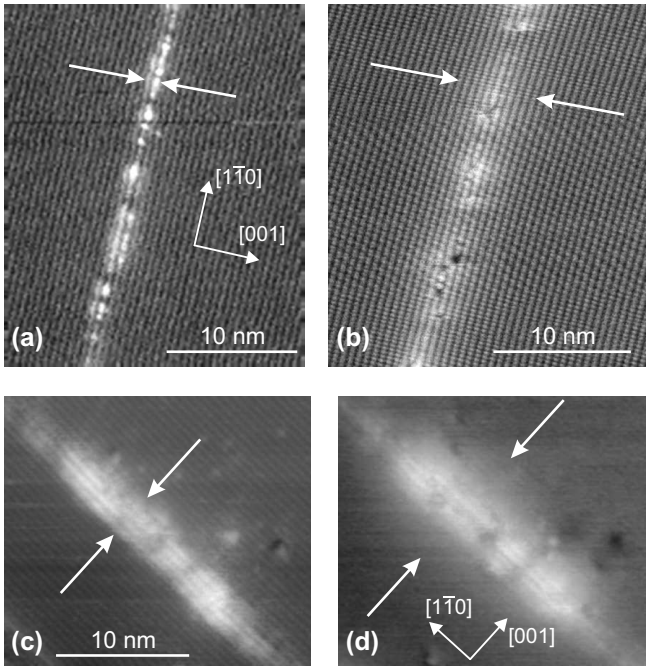

FIG. 1: XSTM images of GaSb/GaAs nanostructures, acquired at both bias polarities: (a) Filled-state image of a QW, taken at a sample bias $V_S = -1.8$ V, and (b) empty-state image of the same QW, taken at $V_S = +2.3$ V. (c) Filled-state image of a ring-shaped QD, taken at $V_S = -2.0$ V, and (d) empty-state image of the same QD, taken at $V_S = +2.0$ V. Tunneling currents are (a, b) 100 pA and (c, d) 80 pA.

the GaSb layer is much smoother, extending over more than ten atomic chains (also marked by arrows). This broadening behavior was found for different samples and is independent of the bias level. Only the tip-height variation at the GaSb QW showed a moderate bias dependence: For negative sample bias varying from -2.0 to -2.5 V it decreases from 1.4 to 0.6 Å, and for positive sample bias of $+2.0$ to $+2.5$ V it decreases from 0.8 to 0.4 Å. This trend is typical for the decreasing influence of electronic effects at higher absolute biases.

The same behavior was observed for GaSb/GaAs QDs, as shown in Fig. 1(c, d). These QDs are generally characterized by a ring shape, but the one shown here was cleaved off center, resulting in a cross-section with a rather compact appearance[28,29]. The imaged QD consists of slightly diluted GaSb and has a baselength of 16.5 nm with a height of four atomic chains or about 2.5 nm[28,29]. While the corresponding contour of the cleaved QD and especially its height are sharply defined in the image with negative sample bias [Fig. 1(c)], upon positive bias imaging the same QD appears fuzzy and surrounded by a brighter region

[Fig. 1(d)].

IV. DISCUSSION AND SIMULATIONS

A. Model of the contrast mechanism

Applying a negative sample bias, the filled valence band (VB) states of the sample are imaged, which can be attributed to the group-V atoms. At positive sample bias, in contrast, the empty conduction band (CB) states are imaged and thus the image contrast is sensitive to the group-III atoms. Thus, the atomic chains in Fig. 1(a, c), resembling the group-V atoms, show a sharp contrast between As and Sb, whereas in Fig. 1(b, d) the Ga atoms are imaged within the cleavage surface.

The bandgap of bulk GaSb amounts to 0.75 eV in contrast to 1.42 eV for GaAs. Therefore in a simple picture a higher tunneling probability could be expected between the XSTM tip and the GaSb region than for GaAs. However, due to the type-II band alignment with a large VB offset but only a small CB offset, the smaller GaSb bandgap should lead to a much brighter image contrast only at negative sample bias, whereas at positive sample bias almost no image contrast should appear. In the case of GaSb/GaAs nanostructures, confined GaSb states within a GaAs matrix have to be considered rather than continuous bulk bands, further influenced by strain[21,32,33]. Nevertheless, also these effects cannot explain the broadened image contrast at positive sample bias, and the band offsets are not sufficient to describe the appearance of the QW.

To explain the observed image contrast, however, also the effect of tip-induced band bending has to be taken into account[20], in combination with the type-II band alignment. Considering these tunneling conditions, we suggest a specific novel contrast mechanism, which is shown schematically in Fig. 2. At negative sample bias, tip-induced band bending at the sample surface region opposite the tip bends the CB minimum at the surface close to the Fermi energy [Fig. 2(a)]. Thus, the GaSb VB states are filled and localized within the QW, and the CB is empty, so that the system remains uncharged [Fig. 2(c)]. When the tip is scanned across the nanostructure, the density of filled states contributing to the tunnel current is much higher in the area sharply defined by the QW than in the surrounding matrix, giving rise to the distinctive contrast observed in Fig. 1(a).

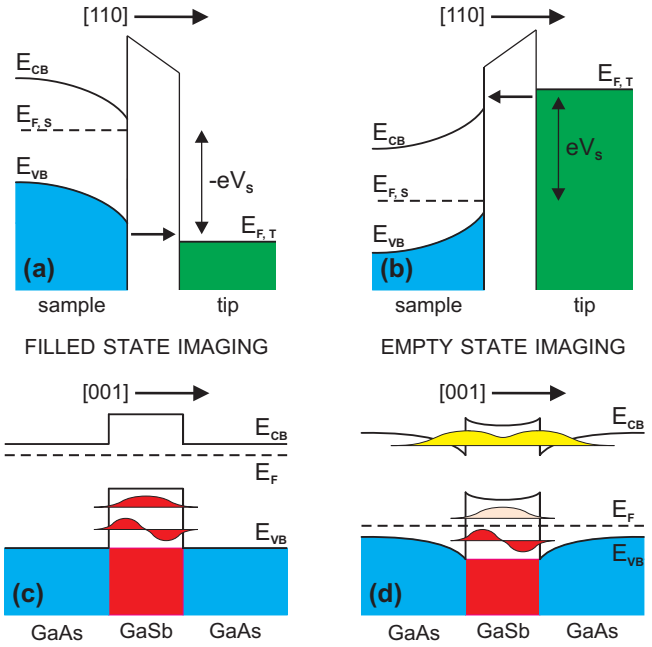

FIG. 2: (Color online) Schematic model of the present XSTM contrast mechanism. (a, b) Tip-induced band bending perpendicular to the cleavage surface. Sample and tip Fermi energies $E_{F,S}$ and $E_{F,T}$ and the applied sample bias voltage are indicated. The GaAs matrix is assumed to be intrinsic, resulting in a bulk Fermi level close to midgap. (c, d) Type-II band alignment along [001]-direction with the consequences of tip-induced band bending. The sample bias is negative for (a) and (c) and positive for (b) and (d), respectively.

The situation is completely different at positive sample bias, where the potential of the tip induces a band bending in the other direction. Therefore, at the sample surface region just opposite the tip the VB maximum of the GaAs material is closer to the Fermi energy [Fig. 2(b)]. The band bending leads to the situation that the hole states within the GaSb may partly lie above the Fermi level and thus get partly depleted. This gives rise to a charging of the nanostructure and therewith to an additional band bending parallel to the cleavage surface along [001]-direction, as shown in Fig. 2(d). Due to this additional band bending, weakly confined electron states appear in the CB of the GaAs surrounding the QW [Fig. 2(d)]. As the STM tip images the empty CB states when it is scanned across the surface at positive sample bias, the tunneling probability gets increased in the range of these Coulomb-confined electron states in the CB, which extend over several nm at both sides of the QW, explaining the smoothly broadened image contrast for the QW seen in Fig. 1(b).

Additionally, directly at the QW tunneling into the depleted GaSb states may occur, but due to the larger energy barrier only at a low probability, so that it can be neglected here. Details of this tunneling path will be published elsewhere[34].

The described effects of tip-induced band bending at type-II QWs can analogously be transferred to the tunneling situation at type-II GaSb/GaAs QDs, as demonstrated in Fig. 1(c, d).

B. Calculation of band bending and electronic height contrast

In order to verify this model of contrast mechanism quantitatively, simulations have been performed of the semiconductor band bending and tunnel current. Band bending is computed by self-consistently solving the Poisson equation for a metallic probe tip near the semiconductor cleavage surface, using a previously described finite element method[35,36]. It should be noted that the tip-induced band bending is not constant at the cleavage surface, but decreases with increasing distance from the tip.

We assume an STM tip with 10 nm radius of curvature and an opening angle for the shank of 90 degrees, separated from the sample surface by 0.8 nm. A 2 nm wide GaSb layer with 0.6 eV VB offset and -0.1 eV CB offset (type II) is assumed, corresponding to a GaSb layer with a slightly increased band gap of 0.9 eV due to compressive strain[37]. Zero doping is used in the semiconductor so that its bulk Fermi level is near midgap, and charge densities are computed in the semi-classical approximation, i.e. with effective-mass bands rigidly following the electrostatic potential energy. Thus, no quantum states in the QW are considered. We use density-of-state effective masses for CB and VB of 0.063 and 0.53 m_e, respectively, for GaAs and of 0.041 and 0.82 m_e for GaSb[37].

The resulting solution closely resembles the one pictured schematically in Fig. 2(c, d). Figure 3(a) shows the computed results for the electrostatic potential energy: The amount of tip-induced band bending at a point on the cleavage surface directly opposite the tip apex is plotted as a function of the tip position along [001] direction with respect to the center of the QW. Note that only the tip-induced band bending, but not the band offsets are shown, even though the latter have been included in solving the Poisson equation. A large variation of the tip-induced potential at the cleavage surface is found as the tip is moved across the QW for positive sample bias, whereas at negative bias the amount of the tip-induced band

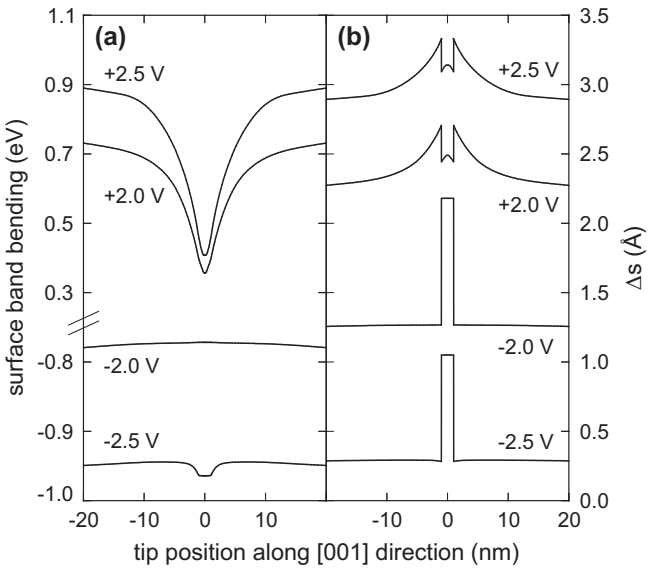

FIG. 3: (a) Calculated electrostatic potential energy shift at a point on the semiconductor surface directly opposite the tip apex, as a function of the tip position with respect to the center of the GaSb QW, for various sample biases. These data are obtained from a three-dimensional solution of the Poisson equation for a tip with radius of curvature of 10 nm. (b) Corresponding constant-current profiles of the tip height, obtained from a semi-classical computation of the tunnel current. The zero level for each profile is arbitrary.

bending is nearly the same for the GaSb QW and the surrounding GaAs layers.

For positive sample bias and tip positions close to the QW the GaSb is (partly) depleted, as pictured in Fig. 2(d), in this way pinning the surface Fermi-level position and limiting the tip-induced band bending. Band bending changes considerably as one moves away from the QW where the Fermi level can approach the GaAs VB edge. In contrast, for negative sample bias, the band bending profiles in the semiconductors are relatively flat, as pictured in Fig. 2(c). Only for larger negative sample bias, when the Fermi level may reach the GaAs CB edge, noticeable changes of the band bending occur at the GaSb QW. It should be noted that this computed band bending is not sensitive to the assumed tip radius of curvature, with very similar results being obtained for radii in the range or 5 – 50 nm (larger radii in general produce larger band bending).

From the band bending, tunnel currents are computed. We follow previous work[20,38] and assume that the current can be obtained as in a planar tunneling computation, but replacing the one-dimensional potential of that problem with the potential $\phi(z)$ from our

finite-element computation along the symmetry axis of the tip. The tunnel current is then given by[39]

$$J = \frac{2e}{h} \int_{-\infty}^{\infty} dE \, [f(E) - f(E - eV_S)] \times \int \frac{d^2 k_\parallel}{(2\pi)^2} \, D_V(E, k_\parallel) \, D_S(E, k_\parallel) \quad , \tag{1}$$

where $f(E)$ and $f(E - eV)$ are Fermi-Dirac occupation factors for the sample and tip, respectively, $k_\parallel$ is the parallel wavevector, and $D_V(E, k_\parallel)$ and $D_S(E, k_\parallel)$ are the transmission terms for tunneling through the vacuum and semiconductor, respectively. Using the Wentzel-Kramers-Brillouin (WKB) approximation and thus neglecting boundary conditions at the semiconductor-vacuum and tip-vacuum interfaces[40], the transmission term for the vacuum, assuming a trapezoidal barrier as shown in Fig. 2(a, b), is approximately given by

$$D_V(E, k_\parallel) = \exp\{-2\kappa s\} \quad , \tag{2}$$

where s is the tip-sample separation and

$$\kappa = \sqrt{\frac{2m}{\hbar^2} \left(\bar{\phi} - E + E_{F_S} + \frac{eV_S}{2} \right) + k_\parallel^2} \quad , \tag{3}$$

where $\bar{\phi}$ is the average work-function of the sample and the tip, and E_{F_S} is the Fermi level at the sample. The integral in Eq. 1 over parallel wavevector is in general restricted by the band structures of both the sample and the tip. However, for a usual metallic probe-tip with a conduction band bottom of about 8 eV below the Fermi level, the restriction will be determined only by the band structure of the semiconducting sample. For effective mass bands, the values of parallel wavevector then extend from 0 to a maximum value of $\left[2m_C^*(E - E_C)/\hbar^2\right]^{1/2}$ for the CB ($E > E_C$) or $\left[2m_V^*(E_V - E)/\hbar^2\right]^{1/2}$ for the VB ($E < E_V$), where m_C^* and m_V^* are the respective effective masses. Here, the density-of-states masses are taken.

Using the WKB approximation, the tunneling transmission term through the semiconductor is given by[20]

$$D_S(E, k_\parallel) = \exp\left\{ -2 \int_A^B \sqrt{\frac{2m_{C,V}^*}{\hbar^2} \, |\phi(z) - E| + k_\parallel^2} \, dz \right\} \, , \tag{4}$$

where $\phi(z)$ is the potential varying perpendicular to the semiconductor surface due to band bending, and A and B determine the boundaries of the tunneling gap. In principle, Eq. 4 should be modified by using either the light-hole effective mass for a VB or an appropriate directional mass for a CB, since these masses best describe the tailing of the wavefunction through the barrier[41]. However, such a correction does not have significant impact on the present calculation, so that we used Eq. 4. Density-of-state effective masses for CB and VB of 0.063 and 0.53 m_e, respectively, for GaAs and of 0.041 and 0.82 m_e for GaSb[37] were used, as mentioned above. An electron affinity of 4.07 eV for GaAs and a metal work function of 4.74 eV were assumed such that flat-band conditions occur for zero sample bias.

Results are shown in Fig. 3(b), where we plot simulated constant-current profiles of the tip height. For negative bias, the profiles display a relatively narrow maximum above the QW, with a height of around 0.8 Å depending on the bias level, which is in good agreement with the experimental observations. For positive sample bias the profiles are quite broad, as a result of the band bending in the surrounding GaAs, with height variations of about 0.4 Å, which also agrees well with the observations.

C. Quantum effects

The main discrepancy between the simulations and the experimental results is a slight depression in the calculated constant-current profile for positive sample bias when the tip is directly above the quantum well. This depression results from a decrease in the number of states available for tunneling in the GaSb due to the type-II CB offset. However, the semi-classical simulations do not take into account the quantum-mechanical tailing of the GaAs CB states into the GaSb, as depicted in Fig. 2(d).

This tailing can be estimated by a simple quantum-mechanical calculation solving the Schrödinger equation, assuming a type-II like CB offset of 0.1 eV, a GaSb barrier width (QW width) of 2 nm, a GaSb CB effective mass of 0.041 m_e, and significant band bending as obtained from the calculated profiles [Fig. 3(a)]: Confined states are found in the GaAs CB surrounding the QW which have a tunneling probability through the GaSb barrier of more than 50%, leading to a situation similar to that shown schematically in Fig. 2(d), so that no significant decrease of the tunneling probability between the semiconductor surface and the tip is obtained when scanning across the nanostructure.

It should be noted that the calculated band bending and tunnel current profiles do not vary significantly if the presumed CB offset is varied between 0 and 0.2 eV of either sign, except for the height of the depression discussed above. Thus, even a type-I behavior of the intermixed GaSbAs QW cannot be excluded, at least as long as there are no confined QW states in the CB, which would change the image contrast drastically towards the well-known behavior of a type-I heterostructure. On the other hand, the results clearly do indicate a large VB offset such that substantial band bending occurs in the GaAs along [001] direction at positive sample bias due to the charging of the QW.

D. Strain relaxation and height profiles

Besides the effects of tip-induced band bending and type-II band alignment, for a full understanding of the XSTM image contrast also the structural contribution has to be considered quantitatively. In the case of strained nanostructures, the structural image contrast is given by strain relaxation upon cleavage[12,14].

In order to calculate this strain relaxation, we used a model based on the linear continuum-mechanical theory of elasticity, applied on discrete atomic positions. The bulk lattice constants and the linear elastic moduli of GaAs and GaSb are taken from Ref.[37]. For the simulation, a cuboid was used with extensions of 48 nm in both [001]- and [1$\bar{1}$0]-directions and 24 nm in [110]-direction, resulting in a total of 2.65×10^6 atoms, resembling a sample with a [110] cleavage surface.

As a starting configuration, this model cuboid contains a GaAsSb QW of 5 ML or 1.5 nm thickness, as evaluated from the XSTM images. During the iterative relaxation, the five side faces are held fixed where the material continues, while all atoms of the cleavage surface and inside the cuboid can relax according to strain energy minimization. Additionally, an offset of the atomic distances is allowed at the GaSb layer along the growth direction. The iterative simulation is stopped when the further expected variation of the atomic positions becomes negligible compared with the resolution of the XSTM experiment. As results of the simulation, both the structural relaxation of the GaAsSb material out of the (110) cleavage surface and the local lattice constant in [001] direction can directly be obtained from the calculated atomic positions. By comparing the calculated local lattice constant at the QW for different given stoichiometries with the experimental XSTM data, as described

in Refs.[7,27,28], the GaSb content of the QW can be determined, amounting here to about 20% GaSb in average, as already mentioned in Section III.

The resulting height profile of the (110) cleavage surface due to the calculated strain relaxation is shown in Fig. 4(a). At the center of the QW it reaches a maximum of 0.17 Å, which is much smaller than typical values for QDs[12,42]. This rather small height relaxation can be explained by the ability of QW to relax its strain partly along [001] direction across the whole crystal, in contrast to the QD case, and further by the strongly intermixed stoichiometry here. Even more important, the simulations show that the strain relaxation is

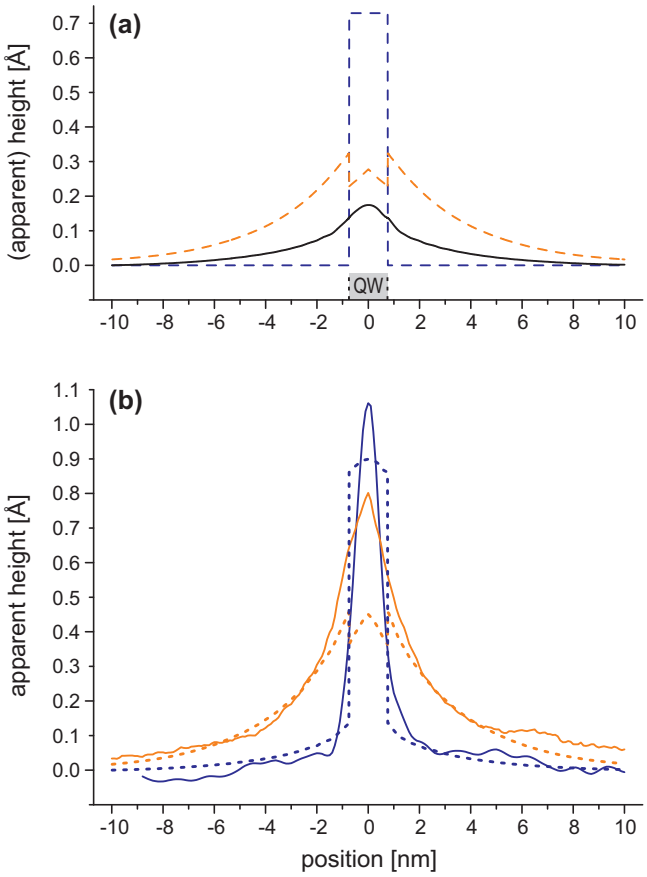

FIG. 4: (Color online) (a) Calculated height profiles across a 1.5 nm thick $GaAs_{0.8}Sb_{0.2}$/GaAs QW, regarding the contributions from either strain relaxation (black solid line) or the electronic height contrast (dashed lines). The position of the QW is indicated. (b) Experimental height profiles (solid lines) and simulated results containing structural and electronic contributions (dotted lines). Dark, blue lines correspond to filled-state imaging at $V_S = -1.8$ V and bright, orange lines to empty-state imaging at $V_S = +2.3$ V.

not restricted to the region of the QW itself, but extends about 10 nm along [001] direction at both sides of the QW. Although this structural protrusion of the cleavage surface beside the QW amounts to less than 0.1 Å, it can well be observed in the XSTM data.

For the same QW geometry and stoichiometry, also height profiles considering the electronic contribution were obtained by calculating the band bending and resulting electronic height contrast as described in Section IV B. While the results shown in Fig. 3 resemble the principle case of a pure and rather thick GaSb layer within GaAs, now the parameters of the simulation are modified in accordance to the precise experimental values, resulting in the dashed curves of Fig. 4(a). For strained GaAsSb/GaAs QWs, the GaAsSb band gap as well as the type-II CB offset increase with QW thickness[21,32,33]. Correspondingly, for the 1.5 nm thick $GaAs_{0.8}Sb_{0.2}$ QW studied here the band gap was estimated to $E_g = 1.1$ eV and a type-II CB offset of 0.15 eV was assumed, in accordance to Refs.[32,33,37,43], resulting in a VB offset of 0.47 eV. Because of the small GaSb content of the QW, GaAs effective masses were used at all positions. The sample bias was chosen to $V_S = -1.8$ V for filled state and $V_S = +2.3$ V for empty state imaging, in accordance to the XSTM images of Fig. 1(a, b).

The total calculated height contrast, considering effects of both band bending and strain relaxation, is obtained by simply adding the corresponding values, plotted as dotted curves in Fig. 4(b). In the same image, experimental height profiles along [001] direction across the $GaAs_{0.8}Sb_{0.2}$ QW, taken at both tunneling polarities, are shown by solid lines. The polarity-dependent appearance with a sharply defined QW at filled-state imaging and a broadly smoothened contrast when imaging the empty states, as discussed in Section IV A, is clearly evident. Good agreement of experiment and simulation is achieved at the sides of the profiles, i.e. at the GaAs at both sides of the QW. While the small increase of the apparent height at the GaAs near the QW for negative sample bias is only due to the structural effect of strain relaxation, the significantly larger increase for positive sample bias is dominated by the additional electronic contrast mechanism, as described in Section IV A.

Directly at the QW, the calculated profiles do not completely match the experimental values. This is already expected since quantum effects were neglected in these calculations, as described in Section IV C, which leads to an underestimation of the height contrast especially for positive sample bias. Additionally, as derived from the XSTM data the Sb composition within the QW is not homogeneous, but decreases from the center to the boundaries of the QW. This effect, however, could not be incorporated into the simulations, so that the

calculated profiles show rather flat curves directly at the QW, in contrast to the sharp peaks in the experimental curves.

V. CONCLUSION AND OUTLOOK

In conclusion, we have found a novel XSTM image contrast mechanism for GaSb/GaAs nanostructures due to tip-induced band bending and the specific type-II band alignment of the material system. The XSTM images show a narrow, sharply defined QW at negative sample bias when the filled states are imaged, and a smoothly broadened contrast at positive sample bias, which is dominated by empty states mainly located in the GaAs material surrounding the QW. Numerical simulations of both band bending and constant-tunnel-current profiles are shown, which are in good agreement with the observations. By additionally calculating the cleavage-induced strain relaxation, the structural and electronic contributions to the image contrast are determined, nicely describing the experimental data.

Extensions to the computation method employed here have also been investigated. The use of the WKB approximation can be avoided by direct numerical integration of the Schrödinger equation through the semiconductor and vacuum regions as in Refs.[36,44]. The results, however, do not significantly differ from the present ones, and for simplicity we maintained the use of the WKB approximation in this work. A more significant extension would be to fully describe the quantum effects for the wave-functions in and near the GaSb QW, as discussed in Section IV C. This was accomplished in Ref.[36] using a fixed form for the wave-function (exponential tails, as applicable to a wide barrier), but that approach cannot be applied to the present problem. A new method is needed, and we have explored using a plane-wave expansion in a supercell geometry. Adequately describing both the long-range band bending effects as well as the short-range quantum well requires a rather large number of k-values. Nevertheless, initial work indicates that this method may be computationally feasible, and future work will focus on this approach.

VI. ACKNOWLEDGMENTS

The authors want to thank L. Müller-Kirsch, U. W. Pohl, and D. Bimberg as well as G. Balakrishnan and D. L. Huffaker for providing the samples. This work was supported

by Project Nos. Da 408/8 and Da 408/13 as well as Sonderforschungsbereiche 296 and 787 of the Deutsche Forschungsgemeinschaft (German Research Foundation) and by the U.S. National Science Foundation (Grant DMR-0503748).

---

* Electronic address: timm@physik.tu-berlin.de

[1] V. Shchukin, N. N. Ledentsov, and D. Bimberg, *Epitaxy of Nanostructures* (Springer, Berlin, 2003).

[2] M. Grundmann, ed., *Nano-Optoelectronics* (Springer, Berlin, 2002).

[3] O. Stier, M. Grundmann, and D. Bimberg, Phys. Rev. B **59**, 5688 (1999).

[4] L.-W. Wang, J. Kim, and A. Zunger, Phys. Rev. B **59**, 5678 (1999).

[5] D. Bimberg, ed., *Semiconductor Nanostructures* (Springer, Berlin, 2008).

[6] W. Wu, J. R. Tucker, G. S. Solomon, and J. S. H. Jr., Appl. Phys. Lett. **71**, 1083 (1997).

[7] H. Eisele, A. Lenz, R. Heitz, R. Timm, M. Dähne, Y. Temko, T. Suzuki, and K. Jacobi, J. Appl. Phys. **104**, 124301 (2008).

[8] R. M. Feenstra, Semicond. Sci. Technol. **9**, 2157 (1994).

[9] A. Lenz, R. Timm, H. Eisele, C. Hennig, S. K. Becker, R. L. Sellin, U. W. Pohl, D. Bimberg, and M. Dähne, Appl. Phys. Lett. **81**, 5150 (2002).

[10] J. M. Ulloa, I. W. D. Drouzas, P. M. Koenraad, D. J. Mowbray, M. J. Steer, H. Y. Liu, and M. Hopkinson, Appl. Phys. Lett. **90**, 213105 (2007).

[11] L. Ivanova, H. Eisele, A. Lenz, R. Timm, M. Dähne, O. Schumann, L. Geelhaar, and H. Riechert, Appl. Phys. Lett. **92**, 203101 (2008).

[12] O. Flebbe, H. Eisele, T. Kalka, F. Heinrichsdorff, A. Krost, D. Bimberg, and M. Dähne-Prietsch, J. Vac. Sci. Technol. B **17**, 1639 (1999).

[13] B. Grandidier, Y. M. Niquet, B. Legrand, J. P. Nys, C. Priester, D. Stiévenard, J. M. Gérard, and V. Thierry-Mieg, Phys. Rev. Lett. **85**, 1068 (2000).

[14] H. Eisele, O. Flebbe, T. Kalka, and M. Dähne-Prietsch, Surf. Interface Anal. **27**, 537 (1999).

[15] S. Gwo, K.-J. Chao, C. K. Shih, K. Sadra, and B. G. Streetman, Phys. Rev. Lett. **71**, 1883 (1993).

[16] O. Flebbe, H. Eisele, R. Timm, and M. Dähne, AIP Conf. Proc. **696**, 699 (2003).

[17] R. Timm, H. Eisele, A. Lenz, T.-Y. Kim, F. Streicher, K. Pötschke, U. W. Pohl, D. Bimberg,

and M. Dähne, Physica E **32**, 25 (2006).

[18] R. M. Feenstra, J. A. Stroscio, J. Tersoff, and A. P. Fein, Phys. Rev. Lett. **58**, 1192 (1987).

[19] R. M. Feenstra, G. Meyer, F. Moresco, and K. H. Rieder, Phys. Rev. B **66**, 165204 (2002).

[20] R. M. Feenstra and J. A. Stroscio, J. Vac. Sci. Technol. B **5**, 923 (1987).

[21] F. Hatami, N. N. Ledentsov, M. Grundmann, J. Böhrer, F. Heinrichsdorff, M. Beer, D. Bimberg, S. S. Ruvimov, P. Werner, U. Gösele, et al., Appl. Phys. Lett. **67**, 656 (1995).

[22] K. Suzuki, R. A. Hogg, and Y. Arakawa, J. Appl. Phys. **85**, 8349 (1999).

[23] M. Grochol, F. Grosse, and R. Zimmermann, Phys. Rev. B **74**, 115416 (2006).

[24] M. Geller, C. Kapteyn, L. Müller-Kirsch, R. Heitz, and D. Bimberg, Appl. Phys. Lett. **82**, 2706 (2003).

[25] M. Geller, A. Marent, T. Nowozin, D. Bimberg, N. Akçay, and N. Öncan, Appl. Phys. Lett. **92**, 092108 (2008).

[26] L. Müller-Kirsch, R. Heitz, U. W. Pohl, D. Bimberg, I. Husler, H. Kirmse, and W. Neumann, Appl. Phys. Lett. **79**, 1027 (2001).

[27] R. Timm, J. Grabowski, H. Eisele, A. Lenz, S. K. Becker, L. Müller-Kirsch, K. Pötschke, U. W. Pohl, D. Bimberg, and M. Dähne, Physica E **26**, 231 (2005).

[28] R. Timm, A. Lenz, H. Eisele, L. Ivanova, M. Dähne, G. Balakrishnan, D. L. Huffaker, I. Farrer, and D. A. Ritchie, J. Vac. Sci. Technol. B **26**, 1492 (2008).

[29] R. Timm, H. Eisele, A. Lenz, L. Ivanova, G. Balakrishnan, D. L. Huffaker, and M. Dähne, Phys. Rev. Lett., **101**, 256101 (2008).

[30] R. Timm, H. Eisele, A. Lenz, S. K. Becker, J. Grabowski, T.-Y. Kim, L. Müller-Kirsch, K. Pötschke, U. W. Pohl, D. Bimberg, et al., Appl. Phys. Lett. **85**, 5890 (2004).

[31] R. Timm, A. Lenz, H. Eisele, L. Ivanova, K. Pötschke, U. W. Pohl, D. Bimberg, G. Balakrishnan, D. L. Huffaker, and M. Dähne, phys. stat. sol. (c) **3**, 3971 (2006).

[32] M. Peter, K. Winkler, M. Maier, N. Herres, J. Wagner, D. Fekete, K. H. Bachem, and D. Richards, Appl. Phys. Lett. **67**, 2639 (1995).

[33] R. Teissier, D. Sicault, J. C. Harmand, G. Ungaro, G. LeRoux, and L. Largeau, J. Appl. Phys. **89**, 5473 (2001).

[34] R. Timm, A. Lenz, H. Eisele, L. Ivanova, V. Voßebürger, T. Warming, I. Farrer, D. A. Ritchie, and M. Dähne, *to be published* (2009).

[35] R. M. Feenstra, J. Vac. Sci. Technol. B **21**, 2080 (2003).

[36] Y. Dong, R. M. Feenstra, M. P. Semtsiv, and W. T. Masselink, J. Appl. Phys. **103**, 073704 (2008).

[37] Landolt-Börnstein, Semiconductors, in *Numerical Data and Functional Relationships in Science and Technology,* edited by O. Madelung, M. Schulz, and H. Weiss, vol. III/17a in *new series* (Springer, Berlin, 1982).

[38] R. M. Feenstra, Phys. Rev. B **50**, 4561 (1994).

[39] C. B. Duke, *Tunneling in Solids* (Academic Press, New York, 1969), eq. (7.8).

[40] R. M. Feenstra, J. Y. Lee, M. H. Kang, G. Meyer, and K. H. Rieder, Phys. Rev. B **73**, 035310 (2006).

[41] In this case, a factor $\alpha = m^{**}/m_d^*$ must be included multiplying the square of the parallel wavevector, where m^{**} is the respective effective or directional mass and m_d^* is a density-of-states effective mass, in order to properly form the perpendicular component of the energy within the square root.

[42] D. M. Bruls, J. W. A. M. Vugs, P. M. Koenraad, H. W. M. Salemink, J. H. Wolter, M. Hopkinson, M. S. Skolnick, F. Long, and S. P. A. Gill, Appl. Phys. Lett. **81**, 1708 (2002).

[43] I. Vurgaftman, J. R. Meyer, and L. R. Ram-Mohan, J. Appl. Phys. **89**, 5815 (2001).

[44] R. M. Feenstra, S. Gaan, G. Meyer, and K. H. Rieder, Phys. Rev. B **71**, 125316 (2005).

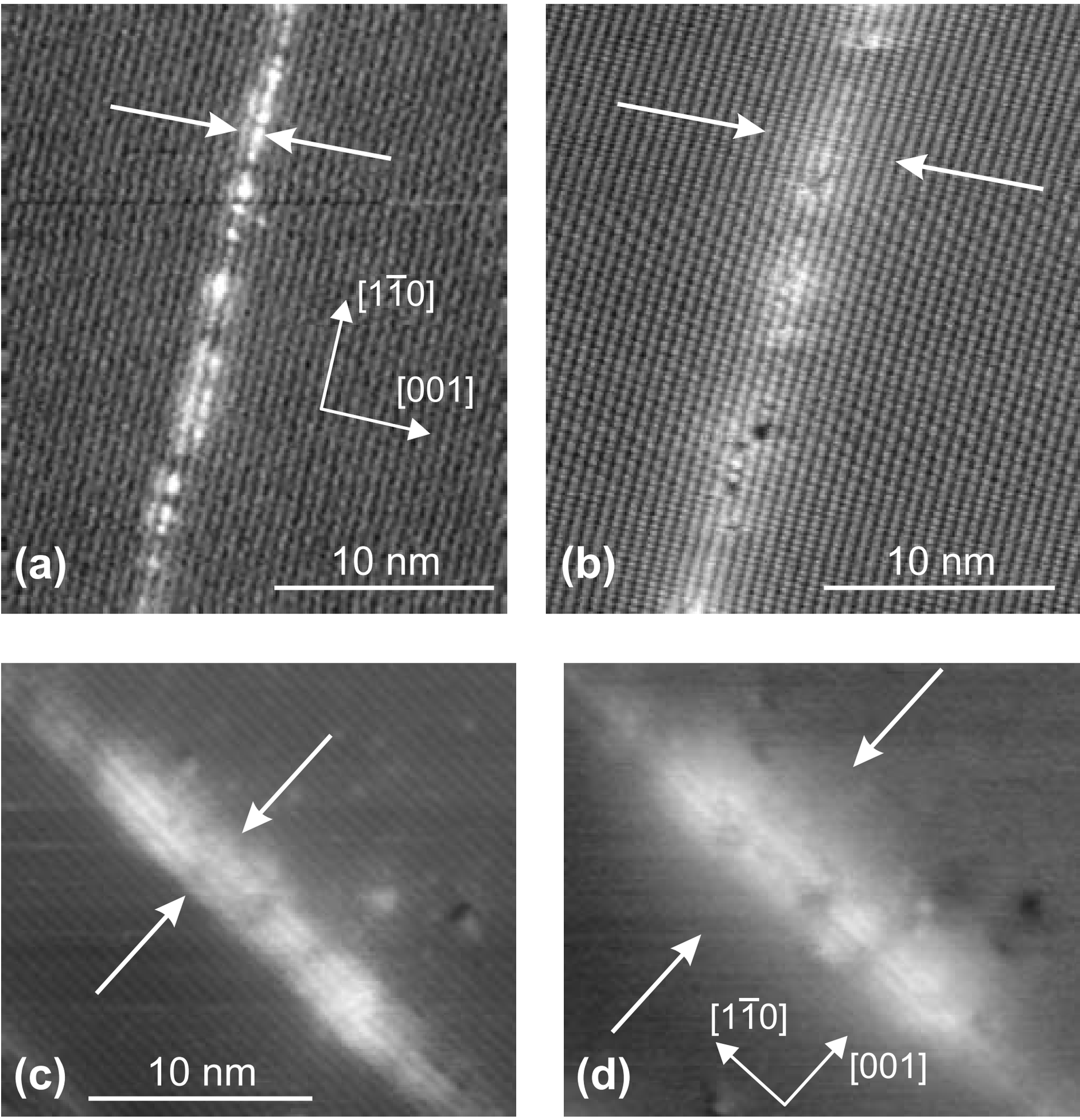
[1$\bar{1}$0]
[001]
(a)
10 nm
(b)
10 nm
(c)
10 nm
(d)
[1$\bar{1}$0]
[001]

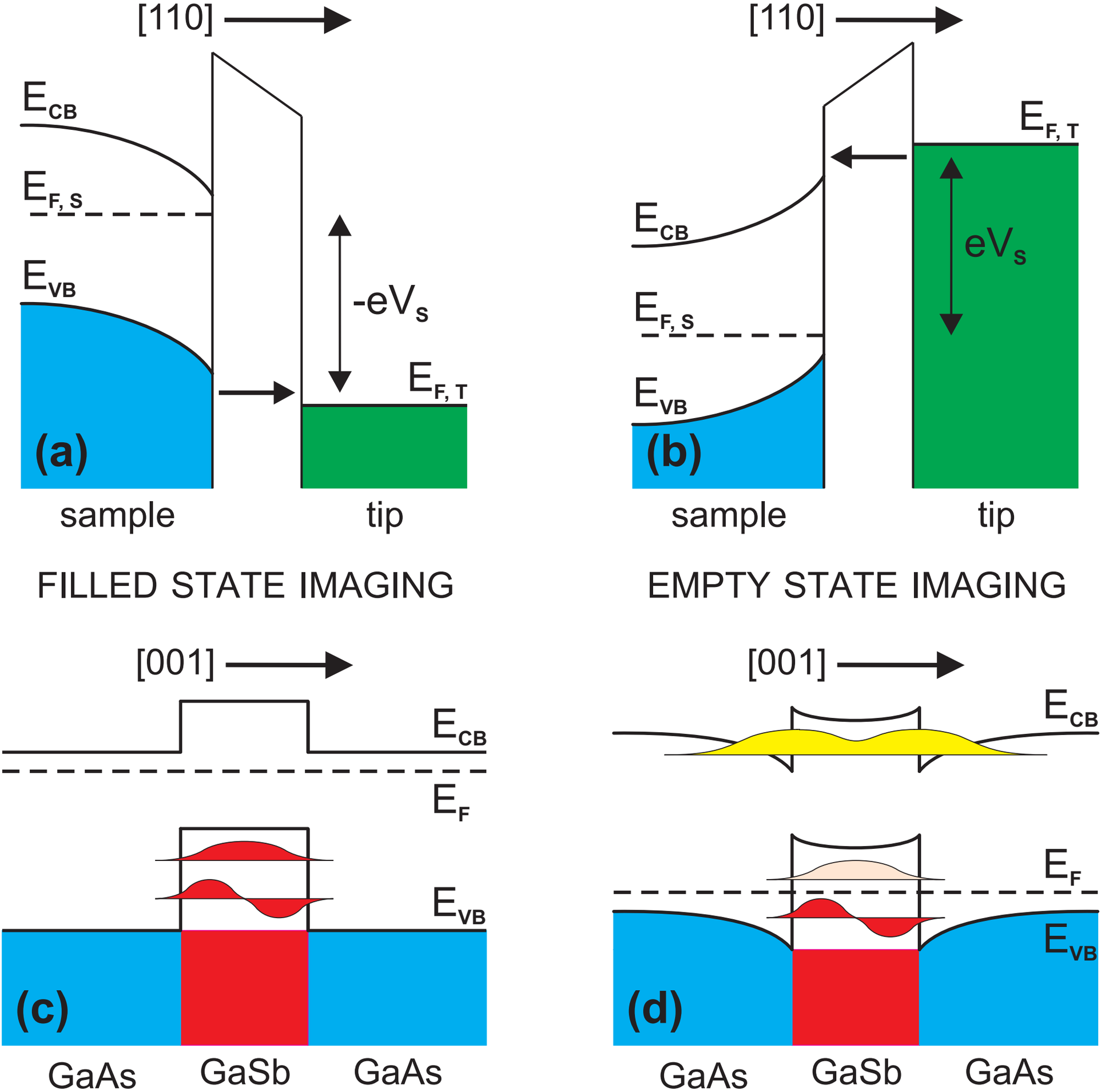
[110]
E_CB
E_F, S
E_VB
-eV_s
E_F, T
(a)
sample
tip
FILLED STATE IMAGING
[110]
E_F, T
eV_s
E_CB
E_F, S
E_VB
(b)
sample
tip
EMPTY STATE IMAGING
[001]
E_CB
E_F
E_VB
(c)
GaAs
GaSb
GaAs
[001]
E_CB
E_F
E_VB
(d)
GaAs
GaSb
GaAs

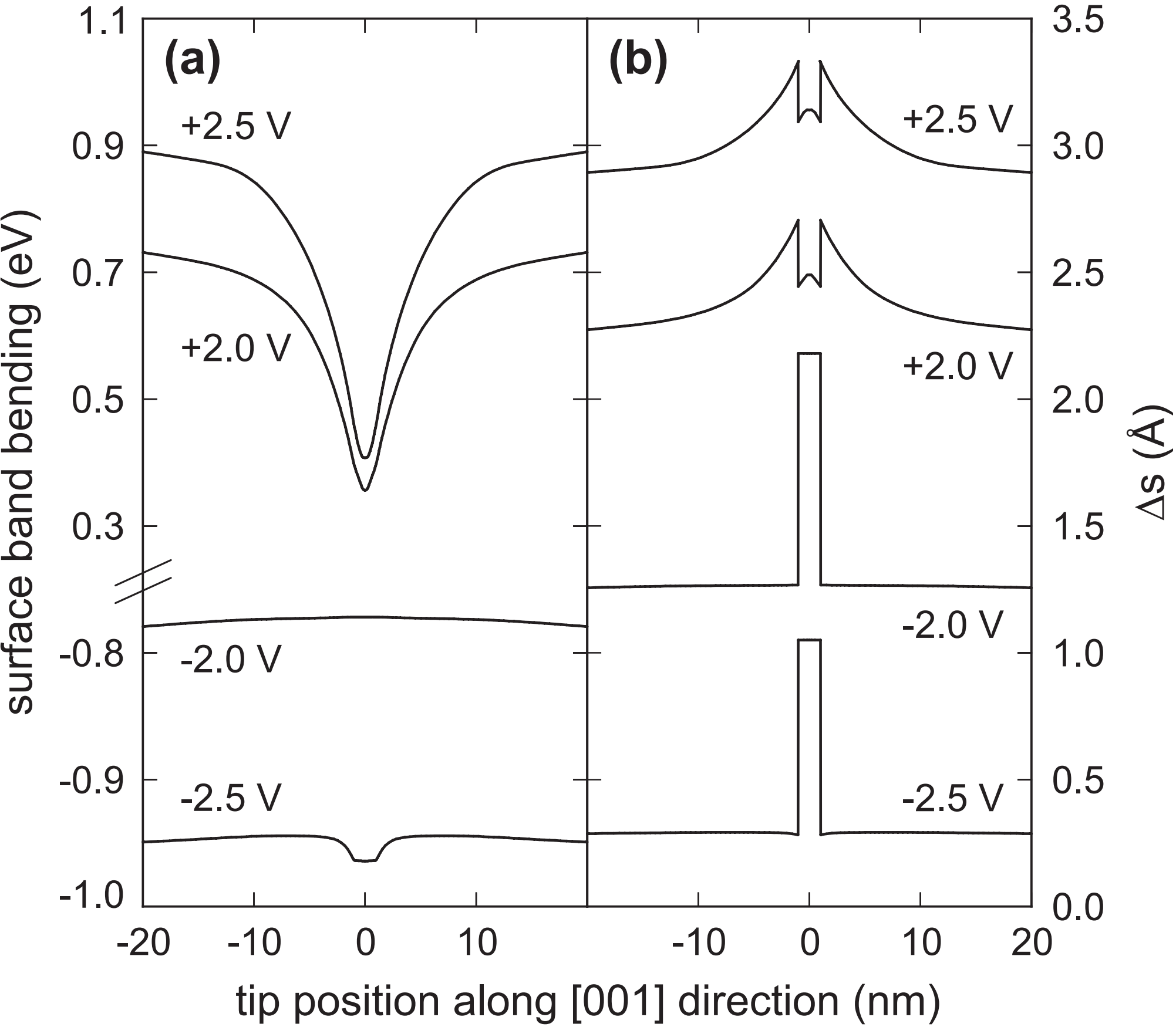
(a)
(b)
+2.5 V
+2.0 V
-2.0 V
-2.5 V
surface band bending (eV)
Δs (Å)
tip position along [001] direction (nm)
1.1
0.9
0.7
0.5
0.3
-0.8
-0.9
-1.0
3.5
3.0
2.5
2.0
1.5
1.0
0.5
0.0
-20
-10
0
10
20

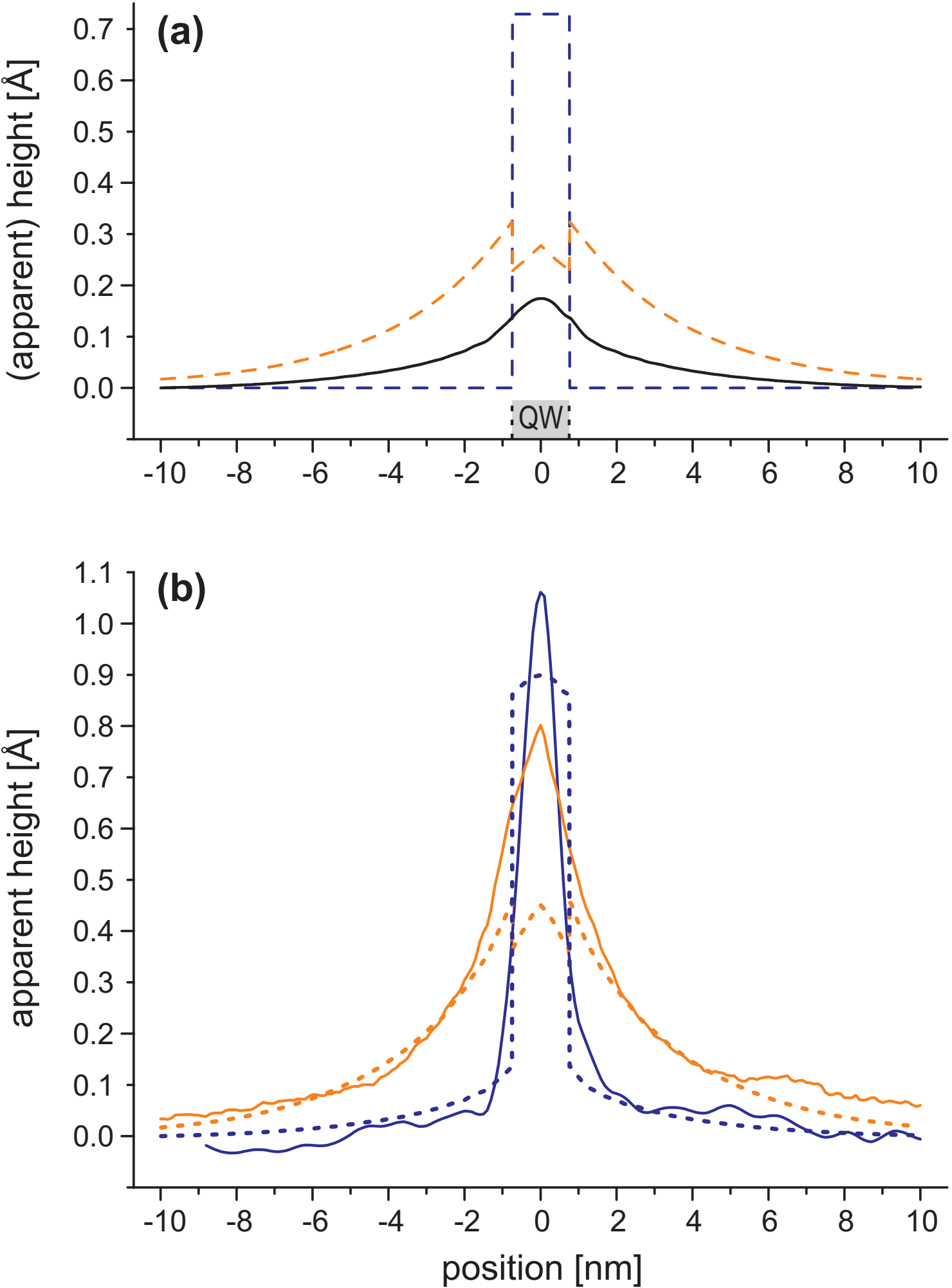
(a)
(apparent) height [Å]
0.7
0.6
0.5
0.4
0.3
0.2
0.1
0.0
QW
-10
-8
-6
-4
-2
0
2
4
6
8
10
(b)
apparent height [Å]
1.1
1.0
0.9
0.8
0.7
0.6
0.5
0.4
0.3
0.2
0.1
0.0
-10
-8
-6
-4
-2
0
2
4
6
8
10
position [nm]